IEEE Access
Multidisciplinary ⋮ Rapid Review ⋮ Open Access Journal

Received 15 February 2023, accepted 5 March 2023, date of publication 16 March 2023, date of current version 23 March 2023.

Digital Object Identifier 10.1109/ACCESS.2023.3257997

RESEARCH ARTICLE

Adaptive Sliding Mode Control for Interleaved *Nx* Multilevel Boost Converter

XIN GE, DONGYI XIAO, YIMIN LU, (Member, IEEE), AND WEI LUO
School of Electrical Engineering, Guangxi University, Nanning 530004, China

Corresponding author: Yimin Lu (y.m.lu@gxu.edu.cn)

This work was supported in part by the National Natural Science Foundation of China under Grant 52167021, and in part by the Key Program of Natural Science Foundation of Guangxi Province of China under Grant 2018GXNSFDA281037.

ABSTRACT Interleaved *Nx* multilevel boost converter (*Nx* MBC) has the advantages of low current stress, high efficiency, and high voltage gain without extreme duty cycle. However, it is difficult to design a controller for interleaved *Nx* MBC due to the high order of state-space equations. A reduced order state-space averaged model of the interleaved *Nx* MBC is proposed to reduce the complexity of the model. For the case of constant power load (CPL), an adaptive sliding mode controller based on nonlinear disturbance observer is designed on the basis of its reduced order state-space averaged model. The nonlinear observer is used to estimate the output power and avoid sampling error caused by interference. In order to ensure the large signal stability of the system, an adaptive law is introduced into the sliding mode controller to suppress the chattering phenomenon. Simulation and experimental results show that the proposed control algorithm has good dynamic regulation characteristics when the CPL and input power supply are disturbed.

INDEX TERMS Interleaved Nx multilevel boost converter, reduced order state-space averaged model, nonlinear disturbance observer, adaptive sliding mode control, constant power load.

I. INTRODUCTION

With the development of renewable energy, DC microgrid has become an option of efficient and convenient energy system [1]. The structure of the traditional DC microgrid is shown in Fig.1. In the DC microgrid, the high gain DC-DC boost converter is usually used as the interface between the renewable energy power generation unit and the DC bus [2]. When the DC-DC converters on the load side are controlled to output constant power, they can be regarded as constant power loads. Normally, the power of the CPL remains constant, and when the output voltage increases, the load current will decrease, so this characteristic is called the negative impedance characteristic [3]. Since the CPL having negative impedance characteristics, it is easy to oscillate when the load changes, which makes the output voltage of the system fluctuate [4]. Therefore, it is particularly important to design a good feedback control strategy to make the high gain DC-DC boost converter operate stably with CPL.

The associate editor coordinating the review of this manuscript and approving it for publication was Zhehan Yi.

In the application of high voltage gain converter, magnetic components such as transformer [5] and coupling inductor [6] are often used to transform the voltage amplitude. However, magnetic components use the principle of electromagnetic induction to transform voltage, which has problems such as low power conversion efficiency and electromagnetic interference [7]. In order to avoid the problems caused by magnetic components, a high gain switched capacitor network *Nx* multilevel boost converter is proposed in [8]. This structure does not require an extreme duty cycle. By increasing the number of stages of the switched capacitor network, the output voltage of the converter is N times larger than that of the conventional boost converter. There are N separate capacitors at the output of this type of topology, which has the function of capacitor voltage self-balancing, so there is no need to adopt a voltage balance control strategy to solve the neutral point potential imbalance problem [9]. However, the inductor current of this topology is relatively large. In [10], the interleaved *Nx* MBC is proposed to reduce the current stress.

To control *Nx* MBC, a reduced order state-space averaged model is proposed in [11]. The transfer function model of

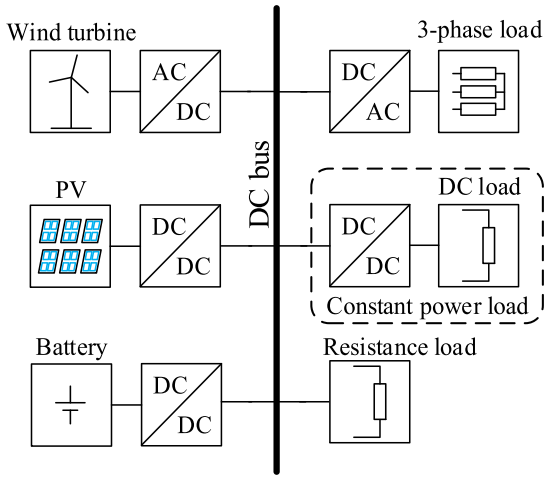

FIGURE 1. DC microgrid structure.

Nx MBC is established in [12], and an improved PI controller is designed based on this model. In [13], an adaptive backstepping controller with extended nonlinear disturbance observer (NDO) is designed for single-phase *Nx* MBC with CPL.

In the control of converter with CPL, ref. [14] proposed a method to counteract the negative impedance characteristics of CPL by adding passive components. But adding passive components will increase the loss of the system and reduce the conversion efficiency. Therefore, the active damping method is introduced to improve the stability of the system with CPL [15], [16], [17], [18], [19]. In [15], a control strategy of active damping adjustment is proposed, in which supercapacitors are used to respond to load changes quickly. In [16], a virtual negative inductor control based on droop control is proposed, in which the virtual negative inductor is used to enhance the system damping of DC microgrid with CPL and increase the stability of the system. Ref. [17] designed a geometric plane to control the converter with a CPL to operate stably on the geometric plane. In [18], model predictive control is applied to DC-DC converter with CPL. In [19], a nonlinear observer is used to estimate the power of CPL, and a predictive controller based on TS fuzzy model is designed.

The computational complexity of geometric switch plane control and model predictive control limits the application of these methods. Sliding mode control has good robustness to external disturbances and avoids complex calculation process. Therefore, it is often used to control DC-DC converter with CPL. In [20], a backstepping sliding mode adaptive controller is designed by using exact feedback linearization technique to make the boost converter work stably. According to the characteristics of CPL, a nonlinear surface sliding mode control method is proposed in [21]. In [22], the voltage error integral term is used to design the sliding surface, and an integral sliding mode controller is designed. Aiming at the problem that the measured power of CPL will affect the control effect, ref. [23] uses nonlinear observer to observe the power of CPL, which suppresses the measurement error caused by sampling process. In [24], a compound nonlinear controller based on feedforward compensation of nonlinear observer and backstepping design algorithm is proposed. In [25], the sliding mode control (SMC) based on nonlinear observer is proposed for interleaved boost converter with CPL. However, in practical applications, the interference range of the system is uncertain. In order to meet the requirement of eliminate the maximum interference, the switching parameter of the SMC usually takes a larger value, which will cause chattering phenomenon and reduce the robustness of the system [26], [27].

In order to suppress chattering and improve the robustness of the system, a reduced order state-space averaged model of interlevel *Nx* MBC is established in this paper, and on this basis, an adaptive sliding mode controller (ASMC) based on NDO is designed. The rest of the paper is arranged as follows: in Section II, the reduced order state-space model of interleaved *Nx* MBC is proposed. In Section III, an ASMC based on NDO is designed to ensure the large signal stability. The simulation and experimental results are given in Section IV and Section V is the conclusion.

II. INTERLEAVED *NX*MBC REDUCED ORDER STATE-SPACE MODEL

The topology of the interleaved *Nx* MBC is shown in Fig.2. It adopts a multi-phase structure, in which the switches Q_j (j = a, b, c, …, m) are conduct alternately according to a phase difference of $2\pi/M$. The number of inductances is equal to the number of structural phases M. The switched capacitor network is composed of multiple identical switched capacitor units interleaved in parallel. The number of energy storage capacitors is $(MN + N - M)$, in which the capacitors $C_1, C_2, \ldots, C_N$ connected to the load are the separation capacitors, and the subscript N represents the multiple N of the interleaved *Nx* MBC. If the full order model of interleaved *Nx* MBC is used to design the controller directly, it will make the controller design very difficult. Therefore, based on the discussion of the working modes of interleaved *Nx* MBC, this section proposes a reduced order state-space averaged model of interleaved *Nx* MBC to reduce the difficulty of controller design. Take the three-phase interleaved 2*x* MBC as an example for modal analysis. Assuming that the duty cycle d of each switch device is equal and the phase angles of each phase are sequentially different by $2\pi/3$, and there are 8 switching modes of the converter. Use "1" and "0" to represent the "on" and "off" states of MOSFETs, respectively. The switch states of switches Q_1, Q_2 and Q_3 can be expressed as corresponding binary numbers: 001(mode I), 010 (mode II), 011 (mode III), 100 (mode IV), 101 (mode V), 110 (mode VI), 111 (mode VII) and 000 (mode VIII). Fig. 3 shows the equivalent circuits. It can be seen from the figure that when the switch Q_j (j=a, b, c) of a certain phase is turned on, the diode D_{j2} (j=a, b, c) in the middle of the same phase is turned on, and the separation capacitor C_1 charges the capacitor C_j (j=a, b, c) in the same phase. When the switch Q_j (j=a, b, c) of a certain phase is turned off,

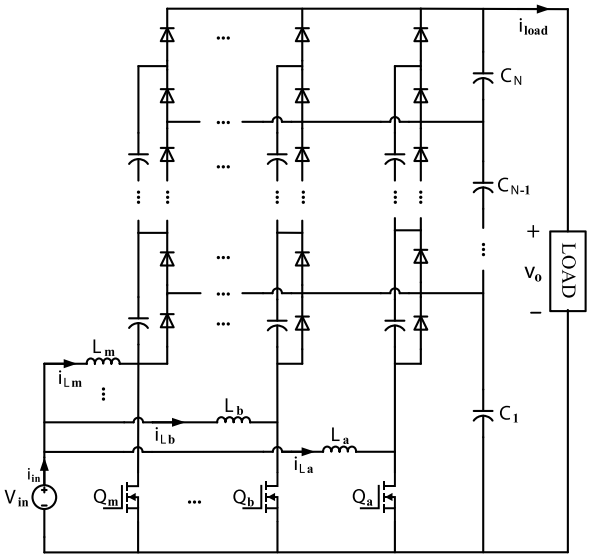

FIGURE 2. Interleaved Nx MBC topology diagram.

the upper and lower diodes D_{j1} and D_{j3} (j=a, b, c) of the same phase are turned on, and the capacitor C_j of the same phase is discharged to the separation capacitor C_2. Because of the structural symmetry of the three-phase interleaved $2x$ MBC topology, the equivalent topology of other types of interleaved Nx MBC can be deduced by analogy. Fig.4 shows the main waveforms when the three-phase interleaved $2x$ MBC works in a steady state under different duty cycles d. When $0 < d \leq 1/3$, the converter operates at the mode of I, II, IV and VIII. When $1/3 < d \leq 2/3$, the converter operates at the mode of I, II, III, IV, V and VI. When $2/3 < d < 1$, the converter operates at the mode of III, V, VI and VII.

According to the Kirchhoff's law, the circuit equations of the interleaved Nx MBC can be obtained as

$$\begin{cases} L_a \dfrac{di_{La}}{dt} = V_{in} - (1-d_a)\dfrac{v_o}{N} \\ L_b \dfrac{di_{Lb}}{dt} = V_{in} - (1-d_b)\dfrac{v_o}{N} \\ \vdots \\ L_m \dfrac{di_{Lm}}{dt} = V_{in} - (1-d_m)\dfrac{v_o}{N} \\ C\dfrac{dv_o}{dt} = \dfrac{1}{\left(1+\sum\limits_{j=a}^{m} d_j\right)} \cdot \left(\sum\limits_{j=a}^{m}\left(1-d_j\right) i_{Lj} - i_{load}\right) \end{cases} \tag{1}$$

where v_o is the output voltage, i_{Li} is the current flowing through the inductor L_i (i = a, b, …, m), and d_j (j = a, b, …, m) is the duty ratio of the drive signal of the j-th phase switch. Furthermore, the current of resistance load is $i_{loadR} = v_o/R$. Meanwhile, the current of CPL is $i_{loadCPL} = P_{CPL}/v_o$.

To meet the application requirements of low ripple and high power, all the inductors take the same inductance value, and the duty cycle of each switch is also the same ($d_j = d$ for j = a, b, …, m). Therefore, the reduced order state-space averaged model can be obtained from (1):

$$\begin{cases} L_{eq}\dfrac{di_{eq}}{dt} = V_{in} - (1-d)\dfrac{v_o}{N} \\ C\dfrac{dv_o}{dt} = \dfrac{1}{1+d}\left[(1-d)\, i_{Leq} - i_{load}\right] \end{cases} \tag{2}$$

where $i_{Leq} = \sum\limits_{j=a}^{m} i_{Lj}$ is the inductor equivalent current, which is also equal to the total input current i_{in}, and $L_{eq} = L/M$ is the equivalent inductance.

III. CONTROL SYSTEM DESIGN

In order to enable the output voltage to track the reference value when the input voltage and load are disturbed, according to the established reduced order state-space averaged model (2), an adaptive sliding mode controller based on a nonlinear observer is designed. The control system block diagram is shown in Fig.5. The proposed controller includes coordinate transformation, NDO, ASMC and current sharing controller. First, new state variables are obtained through coordinate transformation, and the reduced order state-space averaged model is transformed into Brunovsky's canonical form. Then the duty cycle control signal is generated by the NDO and the ASMC. Finally, the current sharing controller is designed to achieve the purpose of adjusting the output voltage and making the current sharing of each phase inductor.

A. COORDINATE TRANSFORMATION AND DESIGN OF NDO

The interleaved Nx MBC system (2) is a nonlinear system. Coordinate transformation is needed to transform the original nonlinear system to Brunovsky's canonical form to handle the nonlinearity introduced by the CPL [28]. Therefore, define new state variables x_1 and x_2 as

$$\begin{cases} x_1 = \dfrac{1}{2}L_{eq}i_{Leq}^2 + \dfrac{1}{2}\left(NM - M + N\right) C\dfrac{v_o^2}{N^2} \\ x_2 = V_{in}i_{Leq} \end{cases} \tag{3}$$

where x_1 is the total energy of the energy storage components of the system. Therefore

$$\begin{cases} \dot{x}_1 = x_2 + y_1 \\ \dot{x}_2 = w \end{cases} \tag{4}$$

where w is the new control variable, and y_1 can be regarded as an unmeasurable uncertain disturbance:

$$\begin{aligned} y_1 = &-(1-d)i_{Leq}\frac{v_o}{N} \\ &+ \frac{(NM - M + N)\, v_o}{(1+d)\, N^2}\left[(1-d)i_{Leq} - i_{load}\right] \end{aligned} \tag{5}$$

From (4), it can be obtained that the control variable d of the original system has the following relationship with w:

$$d = 1 + \frac{wNL_{eq}}{v_o V_{in}} - \frac{V_{in}N}{v_o} \tag{6}$$

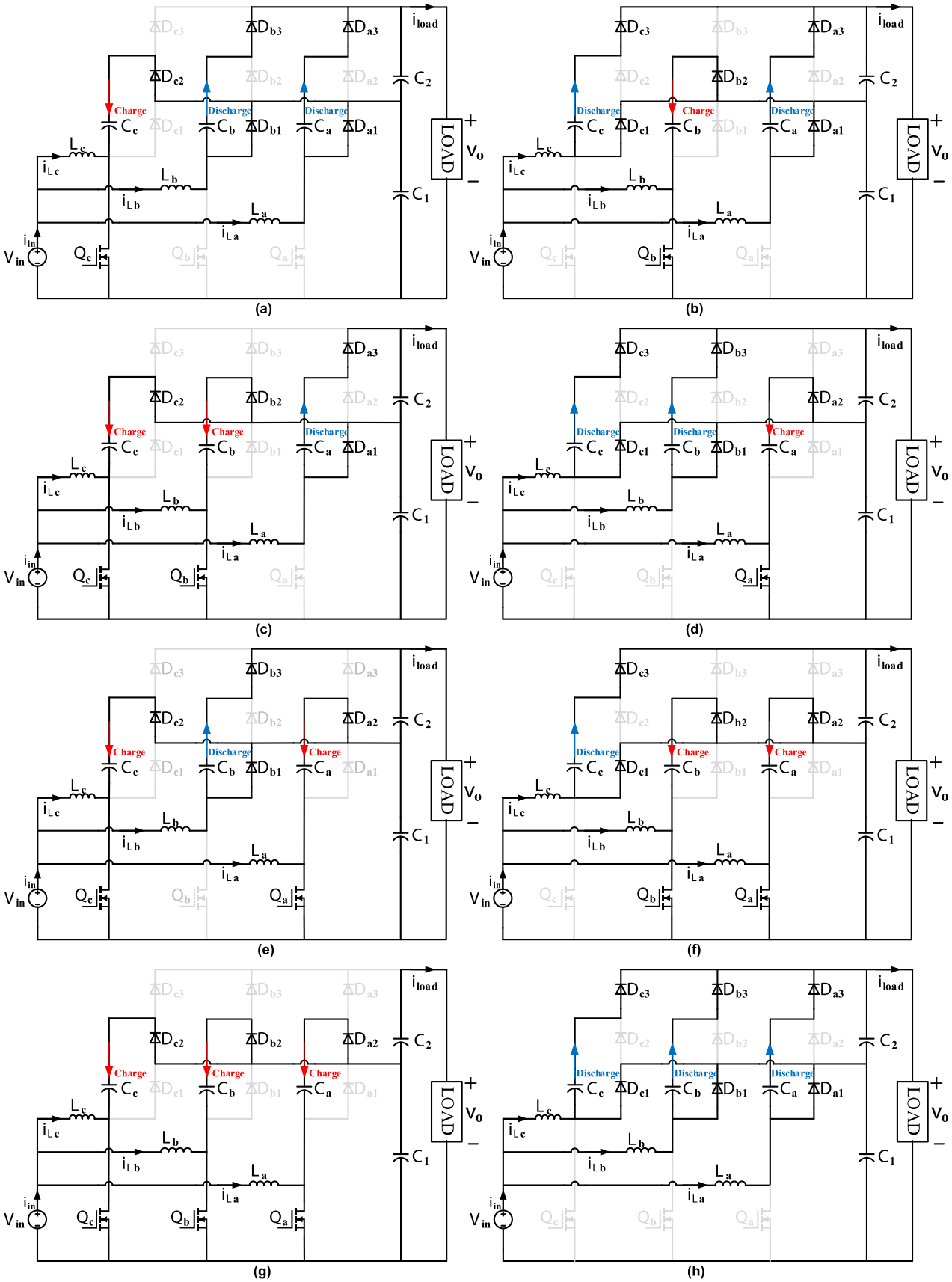

FIGURE 3. Equivalent topological diagram of three-phase interleaved Nx MBC in different working stages. (a)Mode I. (b)Mode II. (c)Mode III. (d)Mode IV. (e)Mode V. (f)Mode VI. (g) Mode VII. (h) Mode VII.

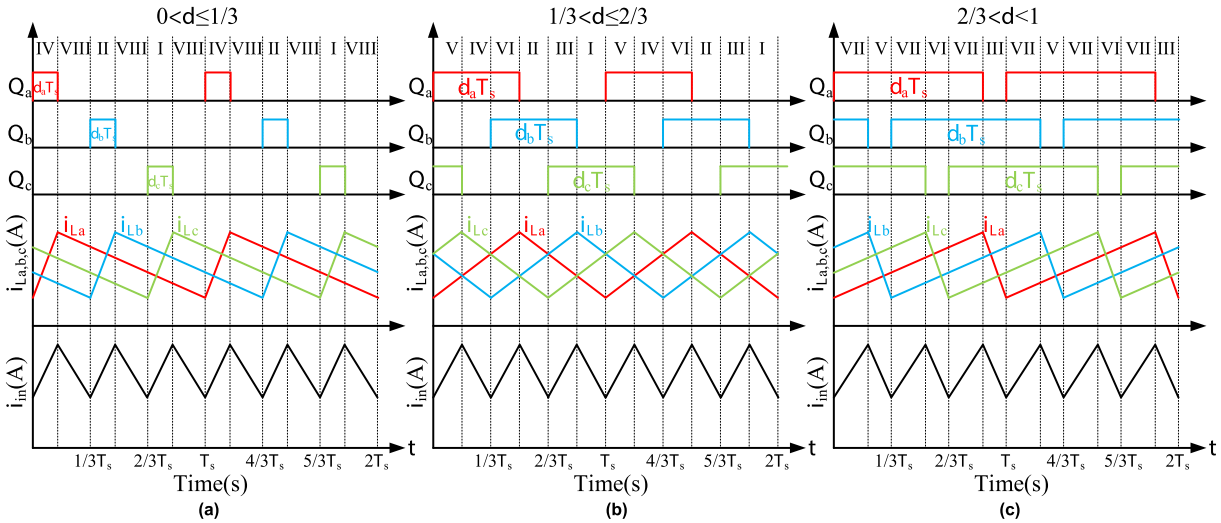

FIGURE 4. Main waveforms of three-phase interleaved Nx MBC in steady-state operation. (a) 0 < d ≤ 1/3. (b) 1/3 < d ≤ 2/3. (c) 2/3 < d < 1.

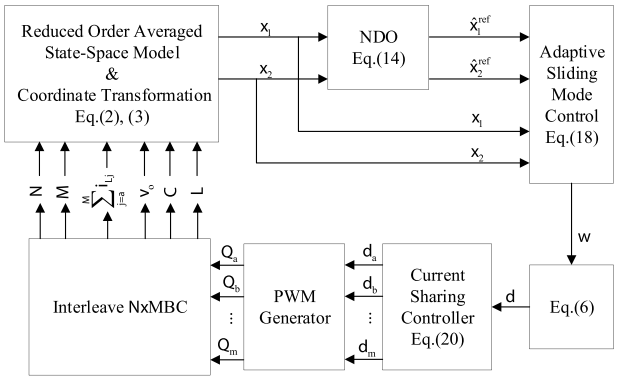

FIGURE 5. Control system block diagram.

According to (5), the reference value of the new system is

$$\begin{cases} x_1^{\text{ref}} = \dfrac{1}{2}L_{\text{eq}}I_{L\text{eq}}^{\text{ref2}} + \dfrac{1}{2}\left(NM - M + N\right)CV_C^{\text{ref2}} \\ = \dfrac{1}{2}L_{\text{eq}}I_{L\text{eq}}^{\text{ref2}} + \dfrac{1}{2}\left(NM - M + N\right)C\dfrac{V_{\text{o}}^{\text{ref2}}}{N^2} \\ x_2^{\text{ref}} = V_{\text{in}}I_{L\text{eq}}^{\text{ref}} \end{cases} \tag{7}$$

where x_1^{ref} is the reference value of x_1, x_2^{ref} is the reference value of x_2, V_o^{ref} is the reference value of output voltage, V_C^{ref} is the reference value of separation capacitors. $I_{L\text{eq}}^{\text{ref}}$ is the equivalent inductor current, which can be expressed as

$$I_{L\text{eq}}^{\text{ref}} = \frac{P_{\text{TP}}^{\text{ref}}}{V_{\text{in}}} \tag{8}$$

where P_{TP} and P_{load} are the input power and load power of the system respectively. If there is no other power loss except the load in the converter circuit, then the reference value of the state variable can be written as

$$\begin{cases} x_1^{\text{ref}} = \dfrac{1}{2}L_{\text{eq}}\left(\dfrac{P_{\text{TP}}^{\text{ref}}}{V_{\text{in}}}\right)^2 + \dfrac{1}{2}\left(NM - M + N\right)C\dfrac{V_{\text{o}}^{\text{ref2}}}{N^2} \\ x_2^{\text{ref}} = P_{\text{TP}}^{\text{ref}} \end{cases} \tag{9}$$

NDO can quickly estimate the change of state variables and serve as a feedforward compensator to increase the accuracy of output regulation. In the actual system, the unmeasurable disturbance y_1 is related to the output power and easily affects the system performance. In order to reduce its influence, a NDO is designed to estimate y_1. The NDO is designed as

$$\begin{cases} \hat{y}_1 = k_1(x_1 - p_1) \\ \dot{p}_1 = x_2 + \hat{y}_1 \end{cases} \tag{10}$$

where k_1 is the observer coefficient, and $\hat{y}_1$ is the estimated value of y_1. Assume that y_1 is bounded and satisfies the following conditions:

$$\begin{cases} y_1(t) \in L_\infty, \dot{y}_1(t) \in L_\infty \\ \lim\limits_{t\to\infty} \dot{y}_1(t) = 0 \end{cases} \tag{11}$$

From (10), the error $\tilde{y}_1$ between the estimated value of the observer and the actual value can be obtained as

$$\begin{cases} \tilde{y}_1 = y_1 - \hat{y}_1 \\ \dot{\tilde{y}}_1 = \dot{y}_1 - \dot{\hat{y}}_1 = \dot{y}_1 - k_1\tilde{y}_1 \end{cases} \tag{12}$$

Substituting $v_{\text{o}} = V_{\text{o}}^{\text{ref}}$ and $d_0 = 1 - NV_{\text{in}}/V_{\text{o}}^{\text{ref}}$ into (5), we can get

$$P_{\text{TP}}^{\text{ref}} = -\hat{y}_1 \tag{13}$$

Substituting (13) into (9), we get

$$\begin{cases} \hat{x}_1^{\text{ref}} = \dfrac{1}{2}L_{\text{eq}}\left(\dfrac{-\hat{y}_1}{V_{\text{in}}}\right)^2 + \dfrac{1}{2}\left(NM - M + N\right)C\dfrac{V_{\text{o}}^{\text{ref2}}}{N^2} \\ \hat{x}_2^{\text{ref}} = -\hat{y}_1 \end{cases} \tag{14}$$

B. ASMC AND CURRENT BALANCE CONTROLLER DESIGN

For the new system after coordinate transformation, the estimated value of the NDO is used as the reference value of the ASMC, and the sliding mode surface is designed accordingly. Then the ASMC is followed by a current sharing controller to

achieve the purpose of current sharing of each phase. Define the error variable as

$$\begin{cases} e_1 = x_1 - \hat{x}_1^{\text{ref}} \\ e_2 = x_2 - \hat{x}_2^{\text{ref}} \end{cases} \tag{15}$$

Define the switching function containing the observations of the NDO as

$$s = ae_1 + e_2 - \dot{\hat{x}}_1^{\text{ref}} \tag{16}$$

where a is a constant. Find the time derivative on both sides of (16), and substitute (4) and (14) to obtain:

$$\dot{s} = a(e_2 - \dot{\hat{x}}_1^{\text{ref}} + \hat{x}_2^{\text{ref}}) + w - \dot{\hat{x}}_2^{\text{ref}} - \ddot{\hat{x}}_1^{\text{ref}} \tag{17}$$

Then, the control law w is designed to ensure that the system output voltage tracks the reference value:

$$w = -a\left(e_2 - \dot{\hat{x}}_1^{\text{ref}}\right) + \ddot{\hat{x}}_1^{\text{ref}} - \dot{\hat{y}}_1 - \bar{k}_{c1}\text{sgn}(s) - k_{c2}s \tag{18}$$

where the control parameter satisfies $\bar{k}_{\text{c1}} > 0$, $k_{c2} > 0$.

Sliding mode control is a switching control. Due to the frequent switching of the control state, the chattering problem caused by it is inevitable. In (18), if the switching parameter $\bar{k}_{\text{c1}}$ is set to a fixed value, the change brought about by the sign function will be amplified by a fixed multiple, and the system will produce chattering. Thus, if a parameter $\bar{k}_{\text{c1}}$ that can be automatically adjusted according to the sliding mode movement is adopted, the effect of chattering can be weakened. When the system state approaches the sliding mode surface, $\bar{k}_{\text{c1}}$ is continuously reduced to decrease the inertia of the motion near the sliding mode surface. When the system state is far away from the sliding mode surface, $\bar{k}_{\text{c1}}$ should be large enough to maintain sufficient speed when approaching the sliding mode surface. The adaptive parameter $\bar{k}_{\text{c1}}$ is designed as follows

$$\bar{k}_{c1} = \lambda \int_0^t |s|\, d\tau \tag{19}$$

Substituting (18) into (6) can obtain the control signal d output by the ASMC.

The purpose of the M-phase interleaved Nx MBC using multiple inductors in parallel is to evenly distribute the input current to the multi-phase inductors, so that the inductor current stress is reduced to $I_{Ljav} = i_{Leq}/M$. In the process of modeling, only the equivalent inductance current i_{Leq} is selected as the state variable, and the current of each inductor is not directly reflected in the model. Because the control signal is dynamic, although i_{Leq} can reach its reference value under the action of the controller, the current of each phase may be unbalanced, which will affect the stable operation of the system. Therefore, a current sharing controller is connected after the ASMC to achieve the current sharing of the M-phase inductor. The current sharing controller is designed as

$$d_{\text{j}current} = K_{Pcurrent}(I_{Ljav} - i_{Lj}) \tag{20}$$

where i_{Lj} is the sampled value of the inductor current of each phase (j = a, b, …, m). $K_{\text{P}current}$ is the proportional coefficient. The final control signal is

$$d_{\text{j}} = d + d_{\text{j}current} \tag{21}$$

C. SYSTEM STABILITY ANALYSIS

The designed controller needs to ensure the stability of the system. The following is based on the Lyapunov stability theory and LaSalle principle to prove the asymptotic stability of the closed-loop control system.

The Lyapunov second method only provides sufficient conditions for stability criteria, which is lead to its conservatism in the estimation of the stability field. In [29], a polynomial Lyapunov function method is proposed for large power system to reduce its conservatism. In circuit system, energy function is usually used as Lyapunov function [30]. Define the first Lyapunov function as

$$V_1 = \frac{1}{2}s^2 \tag{22}$$

Find the time derivative of V_1 and substitute (17) and (18) into (22) to get

$$\begin{aligned} \dot{V}_1 &= s\dot{s} \\ &= s(a\dot{\hat{x}}_2^{\text{ref}} - \bar{k}_{c1}\text{sgn}(s) - k_{c2}s) \\ &\le s(a\tilde{y}_{1\,\max} - \bar{k}_{c1}\text{sgn}(s) - k_{c2}s) \\ &= a\tilde{y}_{1\,\max}s - \bar{k}_{c1}\,|s| - k_{c2}s^2 \end{aligned} \tag{23}$$

where $\tilde{y}_{1\,\max}$ is the maximum error between the observer and the actual value.

When the adaptive law is introduced, the switching function coefficients of the sliding mode controller will change. In order to verify that the system is still asymptotically stable, the second Lyapunov function is selected as

$$V_2 = V_1 + \frac{1}{2\lambda}(K_{c1} - \bar{k}_{c1})^2 \tag{24}$$

where K_{c1} is the upper bound of the adaptive parameter $\bar{k}_{\text{c1}}$, and the time derivative of V_2 can be obtained:

$$\begin{aligned} \dot{V}_2 &= \dot{V}_1 - \frac{1}{\lambda}\left(K_{c1} - \bar{k}_{c1}\right)\dot{\bar{k}}_{c1} \\ &= \sqrt{2}V_1^{\frac{1}{2}}\left(-k_{c2}\,|s| + a\tilde{y}_{1\,\max} - K_{c1}\right) \le 0 \end{aligned} \tag{25}$$

Reasonably set K_{c1} and K_{c2}, when $K_{c1} + k_{c2}\,|s| > a\tilde{y}_{1\,\max}$, $\dot{V}_2 < 0$ can be obtained, then the equilibrium point is asymptotically stable. When $\dot{V}_2 \equiv 0$, then $s \equiv 0$, according to the principle of LaSalle invariance, there are $t \to \infty$, $s \to 0$.

When $s = 0$, according to (16):

$$e_2 = -ae_1 + \dot{\hat{x}}_1^{\text{ref}} \tag{26}$$

where the derivation of e_1 is

$$\begin{aligned} \dot{e}_1 &= e_2 + \tilde{y}_1 - \dot{\hat{x}}_1^{\text{ref}} \\ &= -ae_1 + \tilde{y}_1 \end{aligned} \tag{27}$$

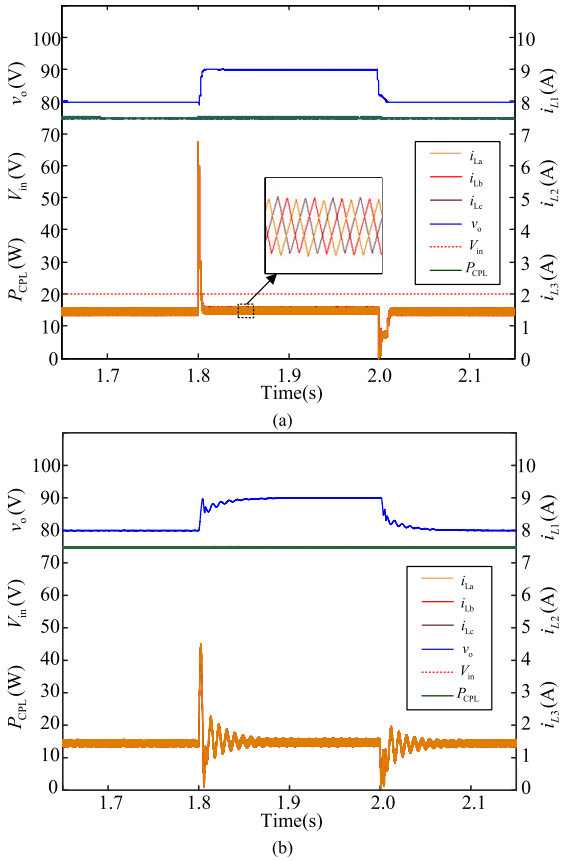

FIGURE 6. Reference voltage variation simulation result graph. (a) ASMC based on NDO. (b) Conventional PI control.

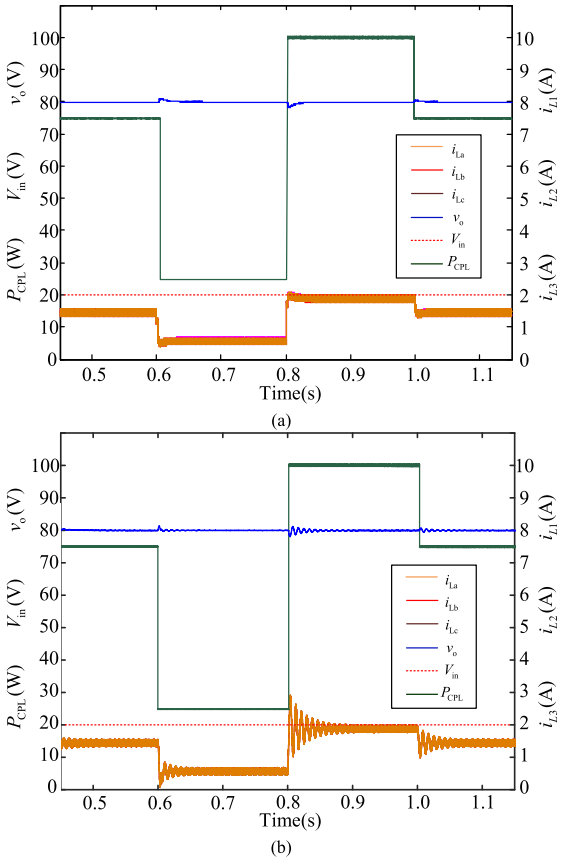

FIGURE 7. Simulation results of constant power load changes. (a) ASMC based on NDO. (b) Conventional PI control.

Let $\dot{e} = [\dot{e}_1, \dot{\tilde{y}}_1]^{\mathrm{T}}$, then:

$$\dot{e} = \boldsymbol{A}e + \boldsymbol{B}y_1 \tag{28}$$

where $\boldsymbol{A} = \begin{bmatrix} -a & 1 \\ 0 & -k_1 \end{bmatrix}$, $\boldsymbol{B} = \begin{bmatrix} 0 \\ 1 \end{bmatrix}$. Since the control variables a and k_1 are both positive, $\boldsymbol{A}$ is the Hurwitz matrix, and the system (28) is asymptotically stable. When $t \to \infty$, $e \to 0, \tilde{y}_1 \to 0$.

IV. SIMULATION AND EXPERIMENTAL RESULTS

In order to verify the effectiveness of the proposed adaptive sliding mode controller based on NDO, a three-phase interleaved $2x$ MBC control system model with CPL was built in MATLAB. The main circuit parameters are designed as follows: the inductance value L_{j} of each phase is 1mH, the switched capacitor C is uniformly selected as 470μF, the constant power load P_{CPL} is initially set to 75W, the input voltage V_{in} is 20V, and the reference output voltage V_o^{ref} is 80V. The controller parameters are selected as follows: adaptive coefficient $\lambda = 10$, nonlinear disturbance observer coefficient $k_1 = 100$, sliding mode control parameters $a = 1200$, $k_{\mathrm{c2}} = 3000$, and the proportional coefficient K_{Pcurrent} in the current balance controller of each phase is taken as 0.2. To verify the performance of the proposed control strategy, a three-phase interleaved $2x$ MBC using a PI controller was designed for comparison. The parameters of this controller are $K_{\mathrm{P}} = 0.005$, $K_{\mathrm{I}} = 0.5$, and $K_{\mathrm{P}current} = 0.2$.

Fig.6 shows the dynamic response waveform of the system when V_o^{ref} changes. Fig.6(a) shows the simulation results of the proposed control strategy. When V_o^{ref} changes from 80V to 90V at 1.8s, the output voltage v_{o} response of the converter is smooth without overshoot. The inductor current rises instantly when the reference voltage changes. Then the three-phase inductor current returns to the steady state after 6ms. In this process, the three-phase current still maintains a current-balance state. At 2.0s, V_o^{ref} recovers from 90V to 80V, the inductor current recovers after a short drop, and the output voltage response is rapid and smooth. The analysis shows that the dynamic response performance of the system is good when V_o^{ref} changes. However, as shown in Fig.6(b), the output voltage response of the PI controller oscillates and the recovery time is longer.

Fig.7(a) shows the response waveform of the system based on the proposed control strategy when the CPL changes suddenly. The CPL is reduced from 75W to 30W at 0.6s. Then the CPL is increased to 100W at 0.8s. Finally, the CPL returns to 75W at 1s. It can be seen from Fig.7 that when the CPL changes, v_{o} returns to the reference value after small fluctuations. The inductor current changes with the CPL. After the transient process, the current sharing state of the inductor has

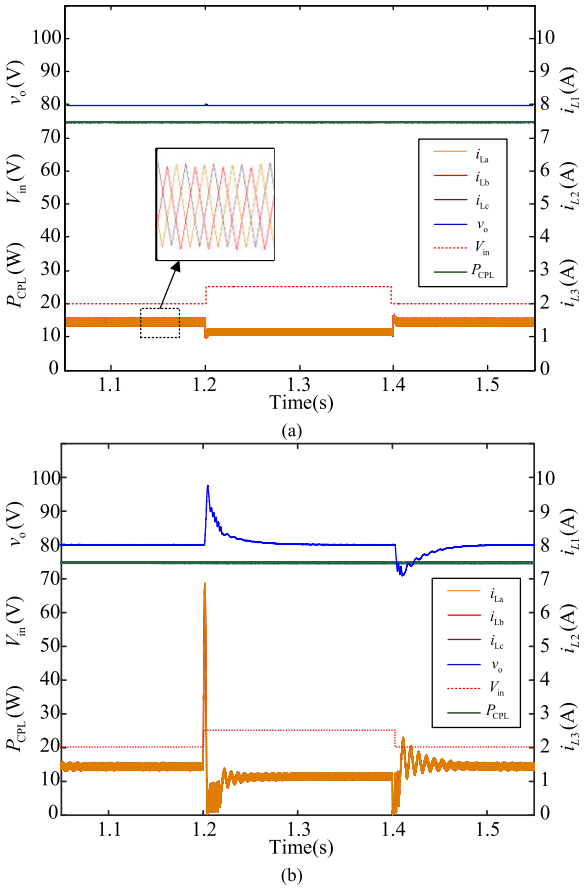

FIGURE 8. Simulation result graph of input voltage change. (a) ASMC based on NDO. (b) Conventional PI control.

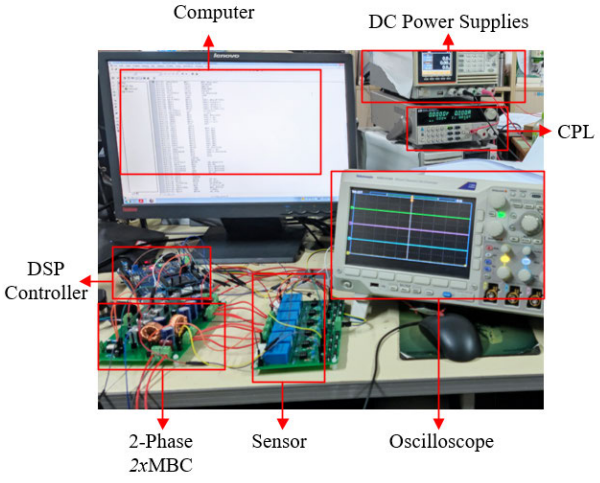

FIGURE 9. Experiment platform.

not been destroyed. Compared with the proposed controller, as shown in Fig.7(b), v_o response of the PI controller brings oscillation when the CPL changes suddenly.

Fig. 8 shows the waveform of the system's response to changes in input voltage V_{in}. Fig. 8(a) shows the simulation results of the proposed control strategy. V_{in} changes from 20V to 25V at 1.2s. Then V_{in} is restored to 20V at 1.4s. During

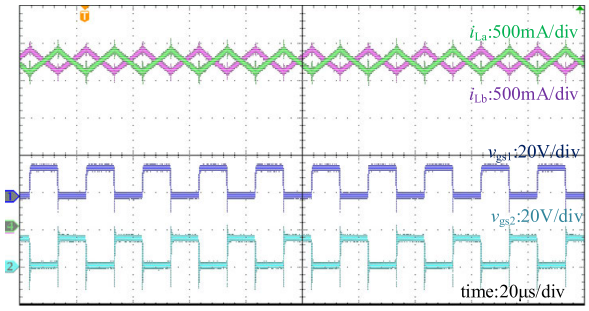

FIGURE 10. Open loop waveform.

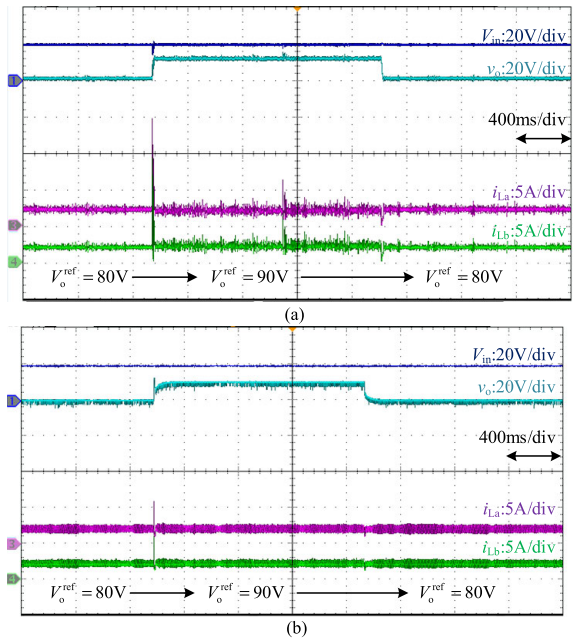

FIGURE 11. Experimental results of reference voltage value jump. (a) ASMC based on NDO. (b) Conventional PI control.

the rise and fall of the input voltage, the output voltages are kept constant. However, the output voltage of the three-phase interleaved 2*x* MBC under PI control oscillates for a long time before it returns to stability.

In order to further verify the effect of the proposed control method, a two-phase interleaved 2*x* MBC experimental platform was designed to test the steady-state and dynamic characteristics of the system. The experimental platform is shown in Fig.9, which is mainly composed of two-phase interleaved 2*x* MBC and driving circuit, sampling and conditioning circuit, DC power supply, DC electronic load, DSP2812, computer and oscilloscope. Two MOSFETs (CSD19536KCS) are used as switches. The driving circuit is composed of TLP250 optocoupler chip. The voltage and current sensors are CHV-25P and CHB-25NP with Hall effect. The main circuit parameters are consistent with the simulation. DSP2812 is used as the controller to realize the proposed control algorithm.

Fig.10 shows the experimental waveforms of two-phase interleaved 2*x* MBC under a fixed duty cycle. When the

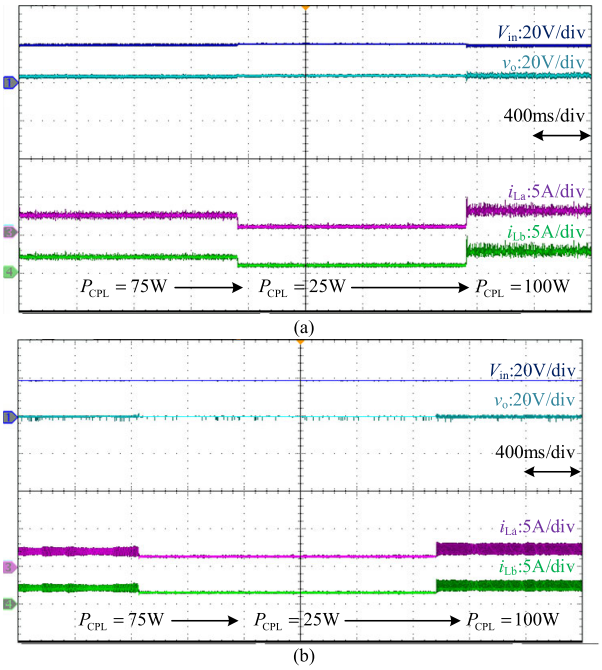

FIGURE 12. Experimental results of constant power load jump. (a) ASMC based on NDO. (b) Conventional PI control.

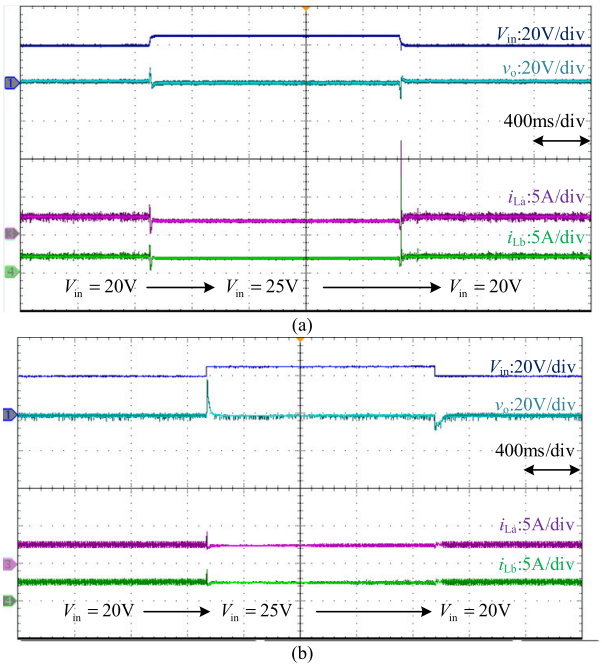

FIGURE 13. Experimental results of Input voltage jump. (a) ASMC Based on NDO. (b) Conventional PI control.

driving signal duty cycle is 0.5, the two MOSFETs are turned on alternately, the inductor current achieves a 180° interleaved waveform. When $P_{CPL} = 75$W and $V_{in} = 20$V, the system voltage output is 80V. The sum of the two-phase inductor current is exactly the theoretical value of the single-phase 2*x* MBC inductor current, which shows that interleaved *Nx* MBC has smaller current stress than single-phase *Nx* MBC.

Fig. 11 shows the voltage and current waveforms when the reference voltage jumps. Under the control of ASMC base on NDO, v_o can be quickly stabilized at a new reference value, while the adjustment time of conventional PI control is longer.

Fig. 12 shows the voltage and current waveforms when the CPL jumps. When the CPL jumps, v_o is basically stable at the reference value under the action of both controllers. But the inductor current ripple under PI control is slightly larger.

Fig. 13 shows the voltage and current waveforms when the input voltage jumps. Compared with the ASMC based on NDO, when V_{in} changes, the conventional PI controller can also make v_o stable at the reference value, but the overshoot is larger. The experimental results show that the ASMC based on NDO has a faster response speed.

V. CONCLUSION

In this paper, the reduced order state-space averaged model of interleaved *Nx* MBC is established to reduce the difficulty of controller design, and an adaptive sliding mode controller based on NDO is designed. The advantages of the proposed control method are:

(1) the chattering of the sliding mode controller is effectively suppressed by adding adaptive parameters to the switching function of the sliding mode controller.

(2) by using the observed value of NDO as the disturbance estimation of feedback control, the adaptability of the control system to the changes of circuit parameters is improved, and the sliding mode chattering is further reduced.

(3) the introduction of NDO reduces the requirements on the accuracy of the sampling circuit and the calculation speed of the controller.

Simulation and experimental results show that the proposed control method makes the system have a fast response speed and robustness. In the process of system modeling and controller design, the parasitic parameters of components are ignored. However, the parasitic parameters of the components exist, and their impact on the control performance will be considered in future research.

REFERENCES

[1] Y.-C. Jeung, D. D. Le, and D.-C. Lee, "Analysis and design of DC-bus voltage controller of energy storage systems in DC microgrids," *IEEE Access*, vol. 7, pp. 126696–126708, 2019.

[2] Q. Xu, W. Jiang, F. Blaabjerg, C. Zhang, X. Zhang, and T. Fernando, "Backstepping control for large signal stability of high boost ratio interleaved converter interfaced DC microgrids with constant power loads," *IEEE Trans. Power Electron.*, vol. 35, no. 5, pp. 5397–5407, May 2020.

[3] Y. Zhao, W. Qiao, and D. Ha, "A sliding-mode duty-ratio controller for DC/DC buck converters with constant power loads," *IEEE Trans. Ind. Appl.*, vol. 50, no. 2, pp. 1448–1458, Mar./Apr. 2014.

[4] T. Dragievi, X. Lu, J. C. Vasquez, and J. Guerrero, "DC microgrids—Part I: A review of control strategies and stabilization techniques," *IEEE Trans. Power Electron.*, vol. 30, no. 7, pp. 4876–4891, Jul. 2016.

[5] J.-K. Kim, S.-W. Choi, C.-E. Kim, and G.-W. Moon, "A new standby structure using multi-output full-bridge converter integrating flyback converter," *IEEE Trans. Ind. Electron.*, vol. 58, no. 10, pp. 4763–4767, Oct. 2011.

[6] H.-C. Liu and F. Li, "Novel high step-up DC–DC converter with an active coupled-inductor network for a sustainable energy system," *IEEE Trans. Power Electron.*, vol. 30, no. 12, pp. 6476–6482, Dec. 2015.

[7] L.-S. Yang, T.-J. Liang, and J.-F. Chen, "Transformerless DC-DC converters with high step-up voltage gain," *IEEE Trans. Ind. Electron.*, vol. 56, no. 8, pp. 3144–3152, Aug. 2009.
[8] J. C. Rosas-Caro, J. M. Ramirez, F. Z. Peng, and A. Valderrabano, "A DC–DC multilevel boost converter," *IET Power Electron.*, vol. 3, no. 1, pp. 129–137, Jan. 2010.
[9] J. Chen, C. Wang, J. Li, C. Jiang, and C. Duan, "An input-parallel–output-series multilevel boost converter with a uniform voltage-balance control strategy," *IEEE J. Emerg. Sel. Topics Power Electron.*, vol. 7, no. 4, pp. 2147–2157, Dec. 2019.
[10] J. C. Rosas-Caro, J. C. Mayo-Maldonado, S. C. Ruben, G. R. Aaron, and C. I. Rodolfo, "A family of DC-DC multiplier converters," *Eng. Lett.*, vol. 19, no. 1, pp. 57–67, 2011.
[11] J. C. Mayo-Maldonado, R. Salas-Cabrera, H. Cisneros-Villegas, M. Gomez-Garcia, and O. Ruiz-Martinez, "Modeling and control of a DC–DC multilevel boost converter," *Lect. Notes Eng. Comput. Sci.*, vol. 4, no. 6, pp. 693–700, 2010.
[12] W. Jiang, S. H. Chincholkar, and C.-Y. Chan, "Investigation of a voltage-mode controller for a DC-DC multilevel boost converter," *IEEE Trans. Circuits Syst. II, Exp. Briefs*, vol. 65, no. 7, pp. 908–912, Jul. 2018.
[13] X. Li, X. Zhang, W. Jiang, J. Wang, P. Wang, and X. Wu, "A novel assorted nonlinear stabilizer for DC–DC multilevel boost converter with constant power load in DC microgrid," *IEEE Trans. Power Electron.*, vol. 35, no. 10, pp. 11181–11192, Oct. 2020.
[14] X. Liu, Y. Zhou, W. Zhang, and S. Ma, "Stability criteria for constant power loads with multistage *LC* filters," *IEEE Trans. Veh. Technol.*, vol. 60, no. 5, pp. 2042–2049, Jun. 2011.
[15] X. Chang, Y. Li, X. Li, and X. Chen, "An active damping method based on a supercapacitor energy storage system to overcome the destabilizing effect of instantaneous constant power loads in DC microgrids," *IEEE Trans. Energy Convers.*, vol. 32, no. 1, pp. 36–47, Mar. 2017.
[16] S. Liu, P. Su, and L. Zhang, "A virtual negative inductor stabilizing strategy for DC microgrid with constant power loads," *IEEE Access*, vol. 6, pp. 59728–59741, 2018.
[17] M. Anun, M. Ordonez, I. G. Zurbriggen, and G. G. Oggier, "Circular switching surface technique: High-performance constant power load stabilization for electric vehicle systems," *IEEE Trans. Power Electron.*, vol. 30, no. 8, pp. 4560–4572, Aug. 2015.
[18] K. Zeinab, S. Qobad, K. Yousef, Y. Meysam, and B. Hassan, "Decentralized model predictive control of DC microgrids with constant power load," *IEEE J. Emerg. Sel. Topics Power Electron.*, vol. 9, no. 1, pp. 451–459, Feb. 2021.
[19] N. Vafamand, S. Yousefizadeh, M. H. Khooban, J. D. Bendtsen, and T. Dragicevic, "Adaptive TS fuzzy-based MPC for DC microgrids with dynamic CPLs: Nonlinear power observer approach," *IEEE Syst. J.*, vol. 13, no. 3, pp. 3203–3210, Sep. 2019.
[20] J. Wu and Y. Lu, "Adaptive backstepping sliding mode control for boost converter with constant power load," *IEEE Access*, vol. 7, pp. 50797–50807, 2019.
[21] S. Singh, D. Fulwani, and V. Kumar, "Robust sliding-mode control of DC/DC boost converter feeding a constant power load," *IET Power Electron.*, vol. 8, no. 7, pp. 1230–1237, 2015.
[22] R. Pradhan and B. Subudhi, "Double integral sliding mode MPPT control of a photovoltaic system," *IEEE Trans. Control Syst. Technol.*, vol. 24, no. 1, pp. 285–292, Jan. 2016.
[23] X. Xu, Q. Liu, C. Zhang, and Z. Zeng, "Prescribed performance controller design for DC converter system with constant power loads in DC microgrid," *IEEE Trans. Syst., Man, Cybern., Syst.*, vol. 50, no. 11, pp. 4339–4348, Nov. 2020.
[24] Q. Xu, C. Zhang, C. Wen, and P. Wang, "A novel composite nonlinear controller for stabilization of constant power load in DC microgrid," *IEEE Trans. Smart Grid*, vol. 10, no. 1, pp. 752–761, Jan. 2019.
[25] W. Jiang, X. Zhang, F. Guo, J. Chen, P. Wang, and L. H. Koh, "Large-signal stability of interleave boost converter system with constant power load using sliding-mode control," *IEEE Trans. Ind. Electron.*, vol. 67, no. 11, pp. 9450–9459, Nov. 2020.
[26] F. J. Chang, E. C. Chang, T. J. Liang, and J. F. Chen, "Digital-signal-processor-based DC/AC inverter with integral-compensation terminal sliding-mode control," *IET Power Electron*, vol. 4, no. 4, pp. 159–167, 2011.
[27] A. Abrishamifar, A. A. Ahmad, and M. Mohamadian, "Fixed switching frequency sliding mode control for single-phase unipolar inverters," *IEEE Trans. Power Electron.*, vol. 27, no. 5, pp. 2507–2514, May 2012.
[28] J. Yang, S. Li, and W.-H. Chen, "Nonlinear disturbance observer-based control for multi-input multi-output nonlinear systems subject to mismatching condition," *Int. J. Control*, vol. 85, no. 8, pp. 1071–1082, 2012.
[29] S. K. Mazumder and E. P. de la Fuente, "Dynamic stability analysis of power network," in *Proc. IEEE Energy Convers. Congr. Expo. (ECCE)*, Montreal, QC, Canada, Sep. 2015, pp. 5808–5815.
[30] S. Bayhan, S. S. Seyedalipour, H. Komurcugil, and H. Abu-Rub, "Lyapunov energy function based control method for three-phase UPS inverters with output voltage feedback loops," *IEEE Access*, vol. 7, pp. 113699–113711, 2019.

XIN GE was born in Zhuzhou, China, in 1996. He received the B.S. degree in electrical engineering from the Hunan University of Science and Technology, Xiangtan, China, in 2018, and the M.S. degree in electrical engineering from Guangxi University, Nanning, China, in 2022. His current research interest includes nonlinear control and its application.

DONGYI XIAO was born in Zhanjiang, China, in 1997. He received the B.S. degree in electrical engineering and automation from the Hunan University of Technology, Zhuzhou, China, in 2019, and the M.S. degree in electrical engineering from Guangxi University, Nanning, China, in 2022. His current research interests include nonlinear control and its applications in power electronics.

YIMIN LU (Member, IEEE) received the B.S. degree in measurement technology and instrumentation from Southeast University, Nanjing, China, in 1992, the M.S. degree in control theory and control engineering from Guangxi University, Nanning, in 2000, and the Ph.D. degree in control theory and control engineering from the South China University of Technology, Guangzhou, China, in 2004. She has been with the School of Electrical Engineering, Guangxi University, since 1992, where she has been a Professor, since 2007. From 2007 to 2008, she was a Postdoctoral Researcher with the Department of Electronic and Electrical Engineering, The University of Sheffield, Sheffield, England, U.K. From 2014 to 2015, she was a Visiting Research Scholar with the Department of Mechanical Engineering and WEMPEC, University of Wisconsin–Madison, Madison, WI, USA. Her current research interests include control theory and its applications in power electronics.

WEI LUO was born in Yongzhou, China, in 1996. He received the B.S. degree in electrical engineering and automation from North Minzu University, Ningxia, China, in 2018, and the M.S. degree in electrical engineering from Guangxi University, Nanning, China, in 2021. His research interests include nonlinear control and applications in power electronics.